Sarcolemmal-restricted localization of functional ClC-1 channels in mouse skeletal muscle

John D. Lueck,[1,3,6] Ann E. Rossi,[1] Charles A. Thornton,[2] Kevin P. Campbell,[3,4,5,6] and Robert T. Dirksen[1]

[1]Department of Pharmacology and Physiology, and [2]Department of Neurology, University of Rochester, Rochester, NY 14642
[3]Department of Molecular Physiology and Biophysics, [4]Department of Internal Medicine, [5]Department of Neurology, and [6]Howard Hughes Medical Institute, Roy J. and Lucille A. Carver College of Medicine, University of Iowa, Iowa City, IA 52246

Skeletal muscle fibers exhibit a high resting chloride conductance primarily determined by ClC-1 chloride channels that stabilize the resting membrane potential during repetitive stimulation. Although the importance of ClC-1 channel activity in maintaining normal muscle excitability is well appreciated, the subcellular location of this conductance remains highly controversial. Using a three-pronged multidisciplinary approach, we determined the location of functional ClC-1 channels in adult mouse skeletal muscle. First, formamide-induced detubulation of single flexor digitorum brevis (FDB) muscle fibers from 15–16-day-old mice did not significantly alter macroscopic ClC-1 current magnitude (at -140 mV; -39.0 ± 4.5 and -42.3 ± 5.0 nA, respectively), deactivation kinetics, or voltage dependence of channel activation ($V_{1/2}$ was -61.0 ± 1.7 and -64.5 ± 2.8 mV; k was 20.5 ± 0.8 and 22.8 ± 1.2 mV, respectively), despite a 33% reduction in cell capacitance (from 465 ± 36 to 312 ± 23 pF). In paired whole cell voltage clamp experiments, where ClC-1 activity was measured before and after detubulation in the same fiber, no reduction in ClC-1 activity was observed, despite an ∼40 and 60% reduction in membrane capacitance in FDB fibers from 15–16-day-old and adult mice, respectively. Second, using immunofluorescence and confocal microscopy, native ClC-1 channels in adult mouse FDB fibers were localized within the sarcolemma, 90° out of phase with double rows of dihydropyridine receptor immunostaining of the T-tubule system. Third, adenoviral-mediated expression of green fluorescent protein–tagged ClC-1 channels in adult skeletal muscle of a mouse model of myotonic dystrophy type 1 resulted in a significant reduction in myotonia and localization of channels to the sarcolemma. Collectively, these results demonstrate that the majority of functional ClC-1 channels localize to the sarcolemma and provide essential insight into the basis of myofiber excitability in normal and diseased skeletal muscle.

INTRODUCTION

Activation of skeletal muscle involves a series of events collectively known as excitation–contraction coupling (Costantin, 1976; Dirksen, 2002; Dulhunty, 2006). The endplate potential generates an action potential that rapidly propagates along the sarcolemma, travels down the transverse tubule (T-tubule) system into the center of the muscle fiber, and subsequently activates voltage sensor dihydropyridine receptors (DHPRs) that trigger calcium release used to drive muscle contraction. The T-tubule system ensures rapid and uniform activation of the entire muscle fiber. However, repeated action potentials during high frequency stimulation can result in significant potassium accumulation within the diffusion-limited T-tubular space (Furman and Barchi, 1977; Kirsch et al., 1977; Almers, 1980; Neelands et al., 2001). Because the potassium equilibrium potential (E_K) sets the skeletal muscle resting potential (-90 mV) (Hodgkin and Horowicz, 1959), an accumulation of extracellular

potassium can result in membrane depolarization sufficient to activate voltage-gated sodium channels to trigger after-discharges (Adrian and Bryant, 1974; Cannon et al., 1993). Sustained bursts of after-discharges result in slowed muscle relaxation (myotonia). A large muscle chloride conductance (G_{Cl}), determined primarily by ClC-1 channels (Lueck et al., 2007a,b), serves to "short circuit" depolarization as a result of potassium accumulation by stabilizing the skeletal muscle resting membrane potential around E_{Cl} (also approximately -90 mV) (Aromataris and Rychkov, 2006; Allen et al., 2008). This powerful membrane potential stabilization effect is possible because G_{Cl} comprises ∼80% of the total resting membrane conductance in mammalian skeletal muscle (Hutter and Padsha, 1959; Aromataris and Rychkov, 2006). The importance of proper ClC-1 channel function in skeletal muscle function is highlighted by the fact that both ClC-1 gene mutations (Pusch, 2002) and aberrant ClC-1 premRNA splicing (Mankodi et al., 2002)

result in myotonic disorders. Given its role in human pathophysiology, the biophysical properties of wild-type (WT) and mutated ClC-1 channels have been extensively characterized in heterologous expression systems. However, a long-standing controversy exists regarding the subcellular localization, sarcolemma or T-tubular system, of chloride channels in native mammalian skeletal muscle.

The first study to investigate the subcellular localization of the G_{Cl} was performed by Hodgkin and Horowicz (1960) in amphibian skeletal muscle. In this hallmark study, the membrane potential was measured during rapid changes in extracellular potassium and chloride ($[K^+]_o$ and $[Cl^-]_o$, respectively). Interestingly, changes in $[Cl^-]_o$ affected the membrane potential more rapidly than $[K^+]_o$. From these findings, it was concluded that K^+-sensitive sites are less accessible than Cl^--sensitive sites. With astonishing forethought, Hodgkin and Horowicz hypothesized that K^+ sites are located in a system of tubules and vesicles of the sarcolemma (Bennett and Porter, 1953; Edwards and Ruska, 1955; Porter and Palade, 1957; Huxley and Taylor, 1958), which are now called the T-tubule system (Andersson-Cedergren, 1959), whereas the bulk of the chloride conductance originates in the sarcolemma. Subsequent measurements of changes in G_{Cl} in frog skeletal muscle (Eisenberg and Gage, 1969) and myotonia in goat skeletal muscle (Adrian and Bryant, 1974) after detubulation also supported the notion that the majority of ClC-1 channels are located in the sarcolemma. Moreover, Gurnett et al. (1995) used biochemical/immunofluorescence approaches and a C-terminal ClC-1 antibody to show that ClC-1 channels localize exclusively to the sarcolemma in mouse skeletal muscle. In contrast, Palade and Barchi (1977) and Dulhunty (1979) found that G_{Cl} was markedly reduced in mammalian skeletal muscle after detubulation using glycerol-induced osmotic shock, consistent with a significant localization within the T-tubule system. More recently, based on mechanically skinned mammalian and amphibian muscle fiber preparations, Lamb and colleagues also concluded that the majority of the G_{Cl} is localized within the T-tubular system (Coonan and Lamb, 1998; Dutka et al., 2008).

The aim of the current study was to determine the subcellular localization of functional ClC-1 channels in mouse skeletal muscle. Results from three complementary approaches (including electrophysiological characterization of macroscopic ClC-1 currents before and after detubulation, immunolocalization of native channels, and in vivo expression of green fluorescent protein (GFP)-tagged ClC-1 channels in DM1 muscle) provide strong evidence that functional ClC-1 channels in adult mouse skeletal muscle reside exclusively within the sarcolemma.

MATERIALS AND METHODS

Preparation of flexor digitorum brevis (FDB) muscle fibers

All animals were housed in pathogen-free areas at the University of Iowa and the University of Rochester School of Medicine and Dentistry and were anesthetized and euthanized using procedures reviewed and approved by the appropriate university committee on animal resources. Skeletal muscle fibers were isolated from FDB muscle obtained from 15–16-d-old and 4-mo-old mice, as described previously (Lueck et al., 2007a,b). In brief, FDB muscles were dissected and mechanically cleaned of connective tissue in a standard Ringer's solution containing (in mM): 146 NaCl, 5 KCl, 2 CaCl$_2$, 1 MgCl$_2$, and 10 HEPES, pH 7.4 with NaOH. Muscles were then shaken for 40 min at 37°C in 1 mg/ml of collagenase A (Roche) dissolved in Ringer's solution. After collagenase treatment, individual FDB fibers were dissociated by gentle trituration using Pasteur pipettes of decreasing bore size. Only fibers exhibiting clear striations and clean surfaces were chosen for electrophysiological recordings. All experiments were conducted at room temperature on fibers obtained within 8 h of isolation.

Macroscopic recordings of ClC-1 currents

The whole cell variant of the patch clamp technique (Hamill et al., 1981) was used to measure macroscopic ClC-1 currents in single FDB fibers, as described previously (Lueck et al., 2007a,b). To ensure complete dialysis with the internal pipette solution (see below), fibers were dialyzed for at least 10 min after the establishment of the whole cell configuration in young fibers and 25 min in adult fibers. The duration of dialysis was determined empirically based on the time required to eliminate subtle alterations in ClC-1 activity as a result of changes in diffusable factors (e.g., pH, ATP, and $[Cl^-]_i$) that may modulate the ClC-1 gating. Ionic currents were compensated for series resistance (>90%), filtered at 2 kHz using an Axopatch 200A amplifier (MDS Analytical Technologies), digitized at 10 kHz using a 16-bit converter, and acquired/analyzed using the pCLAMP 10 software suite (MDS Analytical Technologies).

All ClC-1 currents were elicited using the same voltage protocol. From a holding potential of −40 mV, an initial 250-ms depolarization to +60 mV was used to fully activate ClC-1 channels, followed by a second 500-ms test voltage of variable amplitude (between −140 and +60 mV in 10-mV increments), and then a final 250-ms voltage step to −100 mV. For population studies of detubulated fibers (see below), this voltage protocol was first delivered in the absence and then after the addition of 500 µM 9-anthracene carboxylic acid (9-AC), a blocker of ClC-1 channels. Only experiments with an input resistance of ≥200 MΩ after the addition of 9-AC were included in this study. Offline subtraction of currents recorded in the presence of 9-AC from those recorded in its absence (9-AC–sensitive currents) was used to eliminate residual leak and capacitative currents. After block of ClC-1 currents, total cell capacitance (C_m), uncompensated series resistance (R_s), and the time constant for membrane charging (τ_m) were determined by integration of the capacity transient resulting from the average of five 10-mV depolarizing pulses applied from a holding potential of −80 mV (see Table I for the average C_m, R_s, and τ_m values).

Current density (pA/pF) was calculated for each record to allow for comparison between cells of different sizes. Instantaneous ClC-1 current density was plotted versus membrane test voltage (V_m) and fitted according to:

$$I(V) = (I_{max} - I_0)/(1 + \exp((V_m - V_{1/2})/k)) + I_0, \qquad (1)$$

where I_{max} is the maximum current density at the test potential (V_m), I_0 is a constant offset current, $V_{1/2}$ is the half-maximal activation voltage, and k is a slope factor. Average steady-state current

densities plotted versus V_m were drawn with spline curves. The kinetics of ClC-1 current deactivation elicited at the test potential was determined by fitting the current decay to the following two-exponential function:

$$I(t) = A_1[\exp(-t/\tau_1)] + A_2[\exp(-t/\tau_2)] + C, \qquad (2)$$

where $I(t)$ represents current amplitude at any time t during the pulse, A_1 and A_2 represent the steady-state current amplitudes of each component with their respective time constants (τ_1 and τ_2), and C represents a time-independent current amplitude. For each test potential, the relative contribution of each current amplitude (A_1, A_2, and C) was calculated by dividing the absolute value by the sum of all three components (e.g., $A_1/A_{total} = A_1/[A_1 + A_2 + C]$). The contribution of fast and slow amplitudes and their respective time constants to current deactivation are thought to correspond to ClC-1 protopore and common gating processes, respectively (Accardi and Pusch, 2000).

The voltage dependence of relative ClC-1 channel open probability (Po_{rel}) was calculated from the normalized tail current amplitude elicited in the final voltage step (-100 mV) and fitted according to:

$$Po_{rel}(V) = P_{min} + \left((1 - P_{min})/\left(1 + \exp\left(-\left(V_m - V_{1/2}\right)/k\right)\right)\right), \quad (3)$$

where P_{min} is an offset, V_m is the membrane potential, $V_{1/2}$ is the potential at which $Po(V) = (Po_{max} - P_{min})/2$, and k is a slope factor.

Recording solutions

ClC-1 chloride currents were measured in single FDB fibers from 15–16-d-old mice using an external recording solution consisting of (in mM): 145 TEA-Cl, 10 CaCl$_2$, 10 HEPES, and 0.25 CdCl$_2$, pH 7.4. Low resistance patch pipettes (0.5–0.7 MΩ) were filled with an internal recording solution consisting of (in mM): 110 Cs-aspartate, 30 CsCl, 5 MgCl$_2$, 10 Cs$_2$-EGTA, and 10 HEPES, pH 7.4. Recordings conducted in adult fibers required the use of low chloride internal and external solutions to reduce macroscopic ClC-1 current density. Specifically, the external solution consisted of (in mM): 36.25 TEA-Cl, 108.75 TEA$_2$-SO$_4$, 2.5 CaCl$_2$, 7.5 CaSO$_4$, 10 HEPES, and 0.25 CdCl$_2$, pH 7.4, and an internal solution consisting of 139 Cs-aspartate, 10 CsCl, 5 MgSO$_4$, 10 Cs$_2$-EGTA, and 10 HEPES, pH 7.4. The calculated chloride equilibrium potential (E_{Cl}) was -36 mV in both young and old fibers. Cd^{2+} was used to block L-type Ca^{2+} currents (Fukuda and Kawa, 1977) at a concentration (250 µM) that had no effect on ClC-1 currents (Rychkov et al., 1997; unpublished data).

Detubulation protocol

FDB fiber detubulation was performed using a modification of the formamide addition and withdrawal protocols described previously (del Castillo and Escalona de Motta, 1978; Kawai et al., 1999). For population studies (Figs. 1–3), fibers were bathed in Ringer's solution (see above) supplemented with 1.5 M formamide for 15–30 min. Fibers were then rapidly perfused with a formamide-free external ClC-1 recording solution using bulk perfusion (10 ml/min flow rate). Importantly, fibers were bathed in a very small volume (~500 µl) of formamide-containing solution to ensure that bulk perfusion of external recording solution would produce maximal osmotic shock. Whole cell patch clamp experiments were usually initiated within 10–15 min after perfusion of fibers with external recording solution. Cell capacitance and ClC-1 current magnitude, kinetics, and voltage dependence were determined as described above. Additionally, in some cases ClC-1 currents were measured as long as 3 h after osmotic shock with no significant difference in ClC-1 currents or extent of detubulation. Attempts to detubulate

FDB fibers using conventional glycerol shock treatment (100, 200, and 400 mM glycerol) were unsuccessful because it was not possible to obtain high resistance gigaohm seals in fibers after glycerol shock.

For paired measurements of ClC-1 currents in the same fiber before and after formamide-induced detubulation (Figs. 4–6), cell capacitance was determined from integrating the capacitive transient elicited by a 25-ms voltage step to +100 mV after a 2-s prepulse at +90 mV. A 2-s prepulse was used to ensure that all ClC-1 activation was complete before stepping to +100 mV to avoid ionic current contamination. After control ClC-1 current measurements were taken from naive fibers, recording solution with 1.5 M formamide was slowly perfused into the dish and incubated for 10 min. ClC-1 currents and fiber capacitance were recorded again in the presence of 1.5 M formamide. The solution was then quickly exchanged with formamide-free external recording solution using bulk perfusion. After an additional 7–10 min, ClC-1 currents and fiber capacitance were again recorded. To ensure that a high resistance seal was maintained throughout the experiment, 500 µM 9-AC dissolved in external recording solution was added to block ClC-1 currents. The capacitance calculated from the integral of the capacitative current using a standard +10-mV step from -80 mV after the addition of 500 µM 9-AC (366 ± 20 pF) did not significantly differ from that calculated from the +10-mV step from +90 mV (349 ± 18 pF) delivered in the absence of 9-AC.

To validate formamide-induced detubulation, fiber sarcolemma of naive and formamide-treated fibers was stained for 15 min using the lipophilic fluorescent potentiometric indicator, di-8-butyl-amino-naphthyl-ethylene-pyridinium-propyl-sulfonate (di-8-ANEPPS; 10 µM in Ringer's solution; Invitrogen). Fibers were then imaged after a 30-min incubation in a dye-free Ringer's solution. Di-8-ANEPPS–loaded fibers were excited using a 543-nm laser (605/75-nm emission). Images were acquired using a confocal microscope (Eclipse C1 Plus; Nikon) equipped with a SuperFluor 40× 1.3 NA oil objective. Images were processed and analyzed with National Institutes of Health ImageJ and AutoQuant AutoDeblur & AutoVisualize software packages (Media Cybernetics). A 2-D blind deconvolution was applied to the images for display purposes.

Generation of GFP and GFP-ClC-1-FLAG adenoviral constructs

A cDNA encoding the full-length mouse skeletal muscle chloride channel (ClC-1; available from GenBank/EMBL/DDBJ under accession no. NM_013491) was generated using reverse transcription of mRNA isolated from skeletal muscle of WT mice, as described previously (Lueck et al., 2007b). A novel multiple cloning site including necessary restriction sites was ligated into pCIneo through the use of standard linker reactions (Agilent Technologies). A FLAG-stop sequence was included in the linker between XbaI and NotI restriction sites. 5′ EcoRI and 3′ XbaI restriction sites were added and the initiation methionine and termination codons were removed from ClC-1 using standard recombinant PCR. The ClC-1 PCR product was ligated into the EcoR1/XbaI sites of the modified pCIneo MCS. 5′ KpnI-BsiWI and 3′ EcoRI restriction sites were added to enhanced GFP (Takara Bio Inc.) using PCR. The GFP PCR product was then ligated into the BsiWI/EcoRI sites of the pCIneo MCS. GFP-ClC-1-FLAG was ligated into the KpnI/NotI sites of CMV-pShuttle (Agilent Technologies). GFP-ClC-1-FLAG pShuttle and control pShuttle-IRES-GFP recombinant adenovirus (Ad) were generated according to standard pAd-Easy protocols (Agilent Technologies). Purified adenovirus was isolated using a discontinuous CsCl gradient. Final titers for Ad-GFP and Ad-GFP-ClC-1-FLAG viruses were 10^{10} plaque-forming units (PFU)/ml and 1.6×10^{10} PFU/ml, respectively.

Lueck et al. 599

Expression of ClC-1 channels in mouse skeletal myotubes

Primary cultures of myotubes were prepared from myoblasts obtained from the skeletal muscle of newborn type 1 RYR (RYR1)-null (dyspedic) mice, as described previously (Nakai et al., 1996). Dyspedic myotubes were used as a homologous ClC-1 expression system because they lack endogenous chloride currents (Lueck et al., 2007b) and remain quiescent during nuclear cDNA microinjection. Expression of the GFP and GFP-ClC-1-FLAG constructs was achieved by nuclear microinjection of 0.01 µg/µl cDNA 6–8 d after the initial plating of dyspedic myoblasts.

In vivo adenoviral vector administration

Mice were anesthetized and euthanized by procedures approved by the University Committee on Animal Resources at the University of Iowa and the University of Rochester School of Medicine and Dentistry. 2-d-old WT and transgenic mouse pups expressing ~250 CTG repeats in the 3′ untranslated region of a human skeletal actin transgene (HSA^{LR}) were anesthetized via hypothermia. With a 30-gauge needle, 10 µl of either Ad-GFP or Ad-GFP-ClC-1-FLAG was injected into either the right or left tibialis anterior (TA) muscle. Mice were injected with either GFP or GFP-ClC-1-FLAG adenovirus in the right TA, whereas the other adenovirus was injected in the left TA, thus permitting each mouse to serve as its own control. Pups were then monitored and returned to the mother's cage and kept in quarantine for 21 d. All pups survived adenoviral injections. 3 wk after adenovirus administration, mice were subjected to electromyography (EMG) analysis. General anesthesia was induced by intraperitoneal injection of 100 mg/kg ketamine, 10 mg/kg xylazine, and 3 mg/kg acepromazine. Myotonia was recorded according to published protocols (Mankodi et al., 2000) and scored on a graded scale from 0 (no myotonia) to 3 (myotonic runs after every needle insertion or movement). Importantly, the experimenter was blinded as to which leg received GFP and GFP-ClC-1-FLAG adenovirus before EMG assessment. The excitability of gastrocnemius muscles served as uninjected controls. Mice were euthanized after EMG recordings, and TA muscles were removed and fixed for subsequent immunohistochemical analysis as detailed below.

Immunohistochemical analysis

10-µm-thick cryosections of TA muscles from 21-d-old mice previously injected with GFP and GFP-ClC-1-FLAG adenoviruses were fixed using 4% paraformaldehyde and labeled using a monoclonal RYR1 antibody (1:500; 34C from Developmental Studies Hybridoma Bank, University of Iowa) and a rhodamine-conjugated secondary antibody (1:500; Jackson ImmunoResearch Laboratories, Inc.). Rhodamine and GFP fluorophores were sequentially excited using 543-nm (605/75-nm emission) and 488-nm (515/30-nm emission) lasers, respectively. 3-D fluorescence image stacks (0.5-µm steps) were acquired and averaged ($n = 4$) using a confocal microscope (Eclipse C1 Plus; Nikon) equipped with a SuperFluor 40× 1.3 NA oil objective. Images were processed with AutoQuant AutoDeblur & AutoVisualize software (Media Cybernetics). A 3-D blind deconvolution was applied to the images for display purposes.

Myotubes and FDB fibers isolated as described below were plated on glass coverslips and fixed using 4% paraformaldehyde. A previously described polyclonal ClC-1 antibody (Gurnett et al., 1995) was used at a 1:10 dilution. A monoclonal antibody (VD21; 1:500 dilution) (Leung et al., 1988) and sheep polyclonal antibody (1:200 dilution; Millipore) directed against the DHPR α and β subunit, respectively, were used to visualize the T-tubule system. Alexa Fluor 488 and Alexa Fluor 555 secondary antibodies (Invitrogen) were used to fluorescently label the primary ClC-1 and DHPR antibodies, respectively. Fluorescent images were acquired and averaged ($n = 4$) using an inverted confocal microscope (IX81; Olympus) equipped with a 100× oil objective. Images were processed using FluoView software suite (Olympus).

Statistical analyses

All results are given as means ± SEM, with statistical significance (P < 0.05) determined using two-tailed, paired, or unpaired Student's t test, one-way ANOVA analysis, and Tukey's post-hoc test as appropriate.

Online supplemental material

Fig. S1 demonstrates that exogenously expressed ClC-1 channels containing a bungarotoxin (Btx)-binding site inserted in an extracellular loop are localized to the sarcolemma and not the T-tubule system of mouse FDB muscle. The supplemental text and Fig. S1 are available at http://www.jgp.org/cgi/content/full/jgp.201010526/DC1.

RESULTS

Native ClC-1 channel activity in naive and detubulated FDB fibers

To directly determine the relative contribution of the T-tubule system to total ClC-1 channel conductance in mammalian skeletal muscle, we characterized native ClC-1 channel activity in whole cell patch clamp experiments of mouse FDB fibers before and after the removal of the T-tubule system (Figs. 1–6). We previously demonstrated that macroscopic ClC-1 channel function can be reliably quantified in FDB fibers from young mice
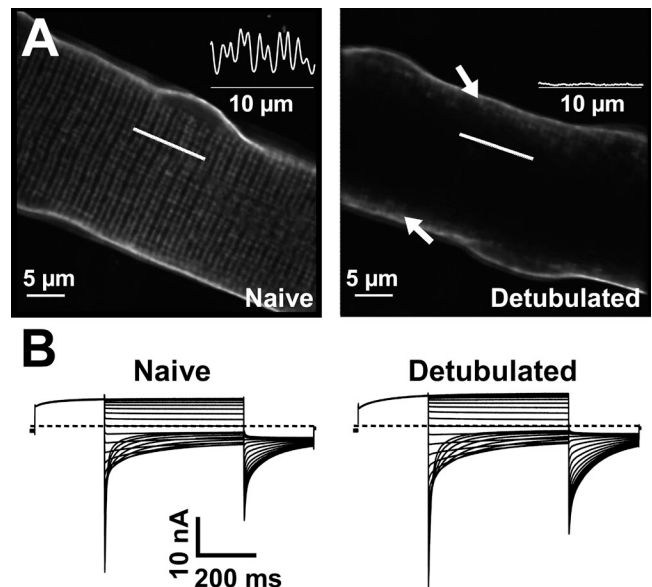

Figure 1. Effect of formamide-induced osmotic shock on di-8-ANEPPS staining and macroscopic ClC-1 currents in mouse FDB fibers. (A) Representative confocal x–y images of di-8-ANEPPS fluorescence in naive (left) and formamide-treated (right) FDB fibers obtained from a 15-d-old mouse. Arrows indicate regions of initial T-tubule invagination that are not fully uncoupled after formamide treatment. (B) Macroscopic whole cell patch clamp measurements of 9-AC–sensitive ClC-1 currents recorded from representative naive (left) and formamide-treated (right) FDB fibers isolated from a 15-d-old mouse.

using the whole cell patch clamp technique (Lueck et al., 2007a,b; Wheeler et al., 2007, 2009). To discriminate between ClC-1 activity as a result of channels residing in the sarcolemma versus the T-tubule system, we used formamide-induced osmotic shock (del Castillo and Escalona de Motta, 1978) to disrupt the continuity between the sarcolemma and T-tubule membrane (i.e., detubulate) in single, acutely dissociated FDB fibers. To validate the extent of detubulation after formamide addition and removal (see Materials and methods for details), naive and formamide-treated fibers were stained with the sarcolemmal potentiometric dye, di-8-ANEPPS. Fig. 1 A (left) shows a confocal image of naive fiber stained with di-8-ANEPPS. The fiber exhibits clear staining of both the sarcolemma and double transverse rows of fluorescence, with an ∼2-μm periodicity (Fig. 1 A, inset), consistent with T-tubule membrane staining (DiFranco et al., 2005, 2007). In contrast, the addition of di-8-ANEPPS to FDB fibers after formamide addition and withdrawal results in only sarcolemmal staining (Fig. 1 A, right). These results confirm that formamide addition and withdrawal result in a massive uncoupling of the T-tubule system from the sarcolemma ("detubulated" FDB fibers).

FDB fibers from 15–16-d-old mice exhibited robust 9-AC–sensitive ClC-1 currents under both control recording conditions (Fig. 1 B, left) and after formamide-induced detubulation (Fig. 1 B, right). Macroscopic ClC-1 currents in naive and detubulated fibers displayed similar characteristic ClC-1 biophysical properties, including inward rectification of the instantaneous current, fast and near complete deactivation at negative potentials, and a reversal potential near E_{Cl}. The average (±SEM) magnitude and voltage dependence of the instantaneous (Fig. 2 A) and steady-state (Fig. 2 B) ClC-1 currents were not different between naive (filled circles) and detubulated (open circles) fibers. Specifically, the average instantaneous ClC-1 current magnitude recorded at −140 mV (Fig. 2 C) was not significantly different between naive (filled squares; −39.0 ± 4.5 nA; $n = 20$) and detubulated (open squares; −42.3 ± 5.0 nA; $n = 18$) fibers. Peak ClC-1 currents recorded at +60 mV were also not different between naive (7.4 ± 1.3 nA) and detubulated (7.8 ± 1.3 nA) fibers. Furthermore, the voltage dependence of relative channel open probability (Po_{rel}) was essentially identical between naive and detubulated fibers (Fig. 2 F and Table I).

The primary effect of formamide-induced detubulation was to markedly reduce total cell capacitance in a manner that results in a parallel increase in ClC-1 current density. This is most clearly illustrated when plotting peak instantaneous ClC-1 current magnitude at −140 mV (Fig. 2 C) and +60 mV (Fig. 2 D) recorded from each naive ($n = 20$; filled circles) and detubulated ($n = 18$; open circles) fiber against its respective membrane capacitance. The average membrane capacitance

was significantly reduced (33%) in the population of detubulated fibers (open squares; 312.0 ± 22.9 pF) compared with that of the naive fiber population (filled squares; 465.3 ± 35.8 pF). Regression analysis of each dataset revealed an increase in the slope of the relationship in detubulated FDB fibers at both −140 mV (Fig. 2 C; $k = −119$ and 187 pA/pF in naive and detubulated fibers, respectively) and +60 mV (Fig. 2 D; $k = 34$ and 54 pA/pF in naive and detubulated fibers, respectively). To ensure that there was no dependence of initial fiber capacitance on ClC-1 current density, fibers of varying size were intentionally chosen for investigation. For a given capacitance, detubulated fibers exhibited a significantly larger ClC-1 current density compared with that
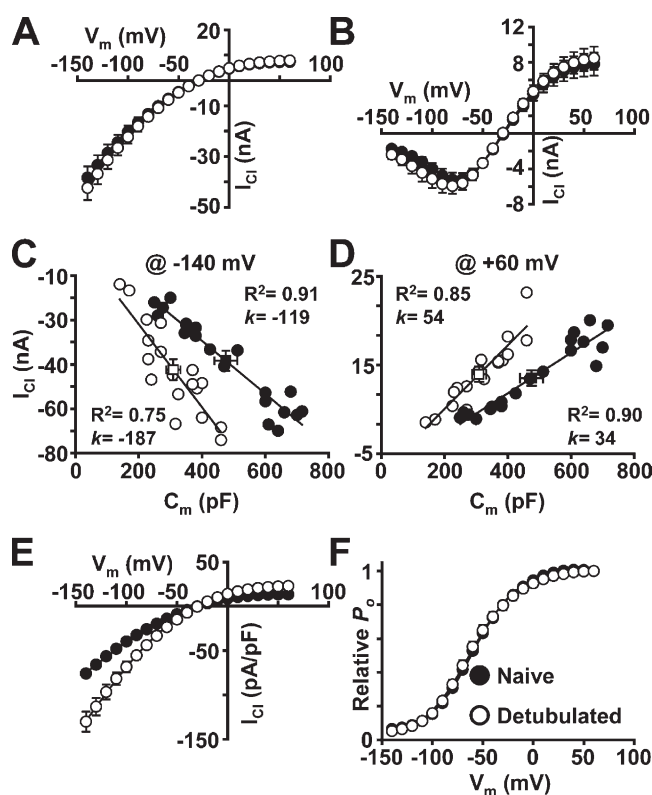

Figure 2. Formamide detubulation does not alter ClC-1 current magnitude or voltage dependence. Average voltage dependence of instantaneous (A) and steady-state (B) ClC-1 current from populations of naive (filled symbols) and formamide-treated (open symbols) FDB fibers from 15–16-d-old mice. Peak instantaneous current amplitude at −140 mV (C) and +60 mV (D) plotted against cell capacitance and fit with a straight line (slope reflecting average current density). Average cell capacitance (±SEM) and current magnitude (±SEM) for naive (filled symbols) and detubulated (open symbols) fibers are shown using square symbols. (E) Average voltage dependence of instantaneous ClC-1 current density of naive (filled symbols) and detubulated (open symbols) FDB fibers from 15–16-d-old mice. (F) Average voltage dependence of relative Po in naive (filled symbols) and detubulated (open symbols) FDB fibers from 15–16-d-old mice. Smooth curves through each Po-V dataset were generated using a modified Boltzmann equation (Eq. 3). Data are mean ± SEM of 20 and 18 control and detubulated fibers, respectively.

TABLE I

Parameters of linear properties and relative open probabilities

	n	Linear properties after 9-AC addition				Po_{rel}	
		C_m	R_m	R_s	τ_m	$V_{1/2}$	k
		pF	*mΩ*	*kΩ*	*μs*	*mV*	*mV*
Population studies							
Naive	20	463 ± 35	244 ± 31	574 ± 27	197 ± 6	-61.0 ± 1.7	20.5 ± 0.8
Detubulated	18	316 ± 22	326 ± 52	500 ± 33	211 ± 10	-64.5 ± 2.8	22.8 ± 1.2
Paired studies							
15–16 d	10	366 ± 20	248 ± 15	541 ± 30	193 ± 5		
4 mo	4	934 ± 40	137 ± 64	302 ± 77	306 ± 94		

All linear properties in the paired studies were obtained after detubulation. *n*, number of fibers; *Cm*, cell capacitance; *Rm*, membrane resistance; *Rs*, uncompensated series resistance; τ_m, membrane time constant; $V_{1/2}$, voltage for one-half activation of *Porel*; *k*, slope factor.

of naive fibers. Comparison of average peak instantaneous current density versus voltage relationships (Fig. 2 E) from naive (filled circles) and detubulated (open circles) fibers further emphasizes the increase in ClC-1 current density (40% at -140 mV) observed in detubulated fibers. Importantly, the absence of a change in raw ClC-1 current magnitude despite a 33% decrease in fiber capacitance as a result of loss of a significant fraction of T-tubule membrane suggests that the majority of functional ClC-1 channels reside within the sarcolemma.

We also evaluated the voltage dependence of channel deactivation in naive and detubulated FDB fibers by fitting the deactivation time course with the sum of two exponentials, as described previously (Lueck et al., 2007b; Wheeler et al., 2007). Across all tested potentials, the relative contribution of the slow (Fig. 3 A), fast (Fig. 3 B), and non-deactivating (Fig. 3 C) gating components and corresponding fast and slow time constants of channel deactivation (Fig. 3 D) did not differ significantly between naive (filled circles) and detubulated (open circles) FDB fibers. When recording large currents from nonspherical cells, the whole cell voltage clamp

technique is vulnerable to incomplete space clamp that can result in distorted recordings (Armstrong and Gilly, 1992). These distortions would be most evident during changes in membrane voltage that induce large amplitude currents, similar to the instantaneous currents elicited at negative step potentials (e.g., -140 mV) reported here. However, we did not observe appreciable changes in ClC-1 current deactivation kinetics at any potential after the disruption of continuity between the sarcolemma and T-tubule membrane, consistent with adequate space clamp in our experiments even before detubulation. In brief, except for an increase in ClC-1 current density as a result of loss of T-tubule membrane capacitance, detubulation had little effect on the macroscopic ClC-1 current magnitude or properties.

Native ClC-1 channel activity before and after detubulation in paired experiments

Results presented in Figs. 1–3 indicate that detubulation does not significantly impact macroscopic ClC-1 current amplitude or properties in separate populations of naive and detubulated fibers. To more directly determine the effect of detubulation, we recorded ClC-1
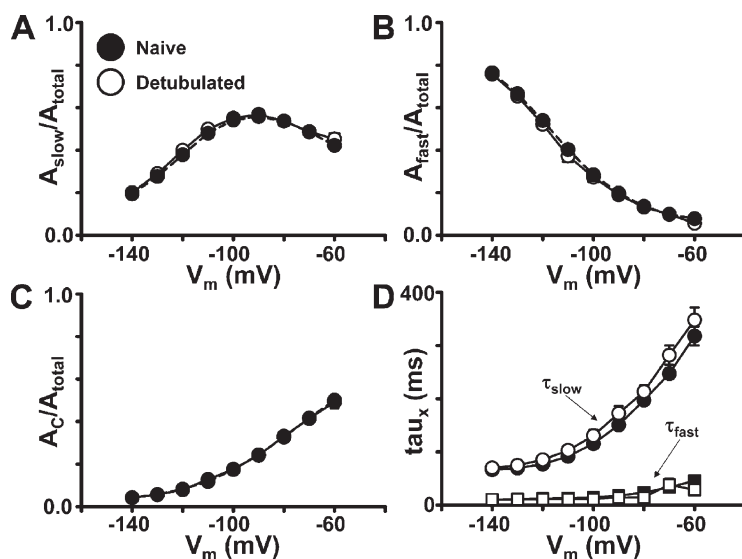

Figure 3. ClC-1 current deactivation is unaffected by formamide detubulation. Average voltage dependence of the relative contribution of slow (A), fast (B), and steady-state (C) components to ClC-1 deactivation in separate populations of naive (filled circles) and detubulated (open squares) FDB fibers from 15–16-d-old mice. (D) Voltage dependence of fast (squares) and slow (circles) time constants of ClC-1 deactivation in naive (filled symbol) and detubulated (open symbol) FDB fibers from 15–16-d-old mice. Data are mean ± SEM from 20 and 18 control and detubulated fibers, respectively.

activity in the same fiber before and after formamide-induced detubulation. For the results presented in Figs. 4 and 5, whole cell patch clamp experiments were conducted in FDB fibers from 15- and 16-d-old mice using the voltage protocol described above. After initial measurements in naive fibers, the formamide detubulation procedure was completed while maintaining the fiber in whole cell voltage clamp ($V_m = -40$ mV). ClC-1 currents were then measured again in the same fiber after detubulation. ClC-1 channels were then blocked by perfusion of 0.5 mM 9-AC, and 9-AC–insensitive currents were recorded. For all fibers, total cell capacitance was measured both before and after detubulation (see Materials and methods). Despite the lengthy protocol requiring several solution changes, we were able to complete multiple experiments in which a >200-MΩ seal resistance was maintained after the final addition of 9-AC. The representative experiment shown in Fig. 4 A demonstrates that currents recorded from a single fiber before (left, black traces) and after detubulation (middle, red traces) exhibit all of the classical ClC-1 biophysical hallmarks (i.e., fast deactivation at negative potentials resulting in current trace crossover, inward rectification, and a reversal potential near E_{Cl}). The striking similarity of the recorded currents is exemplified by superimposing the traces (Fig. 4 A, right), where the ClC-1 currents essentially overlap. ClC-1 currents exhibited nearly identical average steady-state current–voltage relationships before and after formamide treatment (Fig. 4 C), again indicating that few, if any, channels were lost during detubulation. In addition,

the deactivation kinetics of ClC-1 currents recorded from paired naive (open symbols) and detubulated (filled symbols) FDB fibers displays remarkable similarity (Fig. 5) in the contribution of slow (Fig. 5 A), fast (Fig. 5 B), and nondeactivating (Fig. 5 C) components along with the fast (circles) and slow (squares) time constants of gating (Fig. 5 D).

Results presented in Figs. 1–5 are consistent with the majority of functional ClC-1 channels being located in the sarcolemma in FDB fibers from 15–16-d-old mice. However, because the T-tubule system does not reach full structural and functional maturity until at least several weeks postnatal (Beam and Knudson, 1988a; Franzini-Armstrong, 1991), it is possible that sarcolemmal ClC-1 channels could relocate to the T-tubule system sometime after the developmental time point studies in Figs. 1–5. Therefore, we also measured ClC-1 currents before and after detubulation in FDB fibers from 4-mo-old adult mice (Fig. 6). To reduce ClC-1 chloride current magnitude to a level sufficient to achieve a suitable voltage clamp in these experiments, intracellular and extracellular chloride concentrations were reduced to 10.0 and 41.25 mM, respectively. Fig. 6 A shows ClC-1 chloride currents of a representative FDB fiber from a 4-mo-old mouse recorded before (black traces) and after formamide-induced detubulation (red traces). ClC-1 currents in fibers from 4-mo-old mice recorded before and after detubulation exhibited macroscopic properties similar to those observed for fibers from young mice. In addition, formamide addition and withdrawal did not significantly alter macroscopic ClC-1
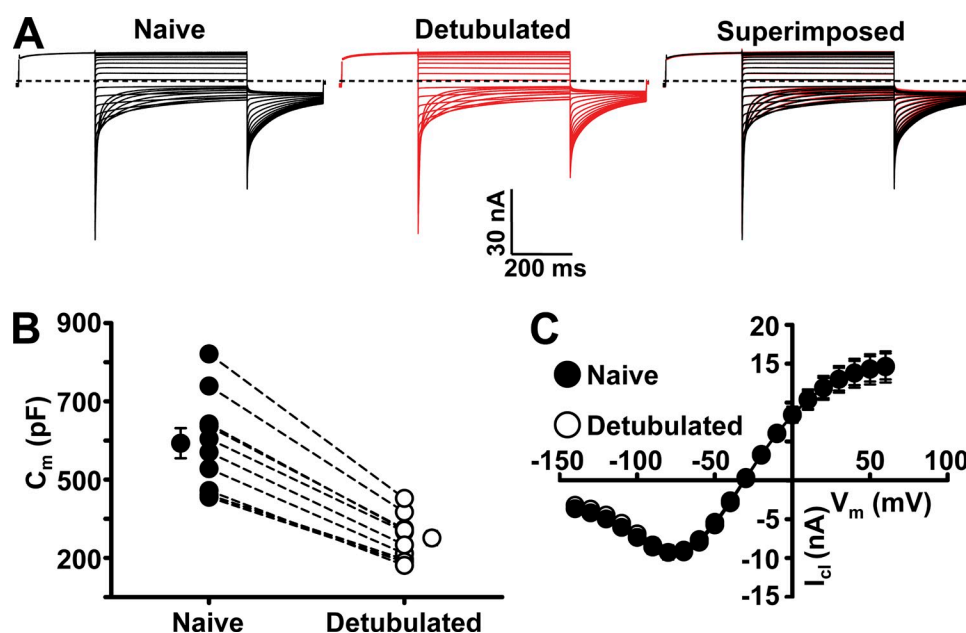

Figure 4. ClC-1 current is similar in FDB fibers before and after formamide detubulation in paired experiments, despite a significant reduction in membrane capacitance. (A) Families of 9-AC–sensitive ClC-1 currents recorded from a representative FDB fiber isolated from a 15-d-old mouse before (black) and after (red) formamide addition and withdrawal. The striking similarity in ClC-1 activity before and after formamide detubulation is emphasized by superimposing the two families of 9-AC–sensitive ClC-1 currents (right). Total cell capacitance for this fiber was reduced from 603 to 352 pF after formamide addition and withdrawal. (B) Average membrane capacitance was significantly reduced 40.6 ± 2% ($n = 10$) in FDB fibers from 15–16-d-old mice after formamide addition and withdrawal. (C) Average voltage dependence of steady-state ClC-1 currents recorded from FDB fibers from 15–16-d-old mice before (filled symbols) and after (open symbols) formamide addition and withdrawal. Data are presented as mean ± SEM ($n = 10$ each control and detubulated fibers).
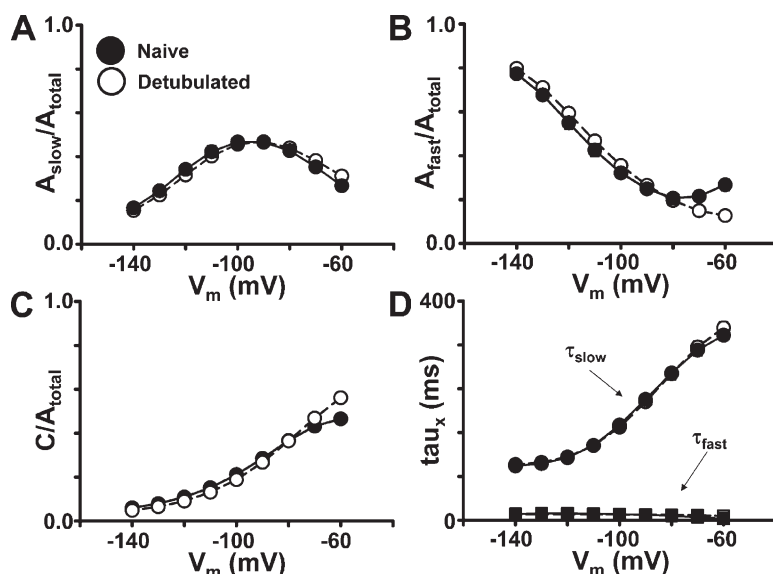
Figure 5. ClC-1 current deactivation is unaffected by formamide detubulation in paired experiments. Average voltage dependence of the relative contribution of slow (A), fast (B), and steady-state (C) components to ClC-1 deactivation in naive (filled circles) and detubulated (open squares) FDB fibers from 15–16-d-old mice in paired experiments. (D) Average voltage dependence of fast (squares) and slow (circles) time constants of ClC-1 deactivation in naive (filled symbol) and detubulated (open symbol) FDB fibers. Data mean ± SEM ($n = 10$ each control and detubulated fibers).

current magnitude or properties, despite a 61% reduction in total cell capacitance (from 2,073 to 815 pF; Fig. 6 B). In four experiments, ClC-1 steady-state current magnitude was not significantly reduced in FDB fibers from 4-mo-old mice after formamide-induced detubulation (Fig. 6 C), in spite of a significant reduction in total cell capacitance (from 2,286 ± 80 pF to 933 ± 80 pF; Fig. 6 D).

Immunofluorescence of native ClC-1 channels in FDB fibers
Careful inspection of the di-8-ANEPPS fluorescence in detubulated fibers (Fig. 1 A, right) suggests that initial segments of the T-tubule were sometimes not completely detached from the sarcolemma, leaving T-tubule "necks" attached in which ClC-1 channels could conceivably

be concentrated, similar to that shown previously for caveolin-3 (Murphy et al., 2009). Previous studies have concluded that native ClC-1 is primarily localized in the sarcolemma based on ClC-1 immunoreactivity in purified sarcolemmal preparations (Gurnett et al., 1995) and ClC-1 immunofluorescence of muscle cross sections (Gurnett et al., 1995; Mankodi et al., 2002; Papponen et al., 2005; Wheeler et al., 2007, 2009). However, preferential concentration of endogenous ClC-1 channels just inside the point of T-tubule invagination would likely have escaped detection in these studies. Accordingly, we conducted high resolution confocal microscopy of endogenous ClC-1 immunofluorescence in single FDB fibers isolated from 4-mo-old adult mice using an antibody directed toward the ClC-1 C-terminus (Fig. 7).
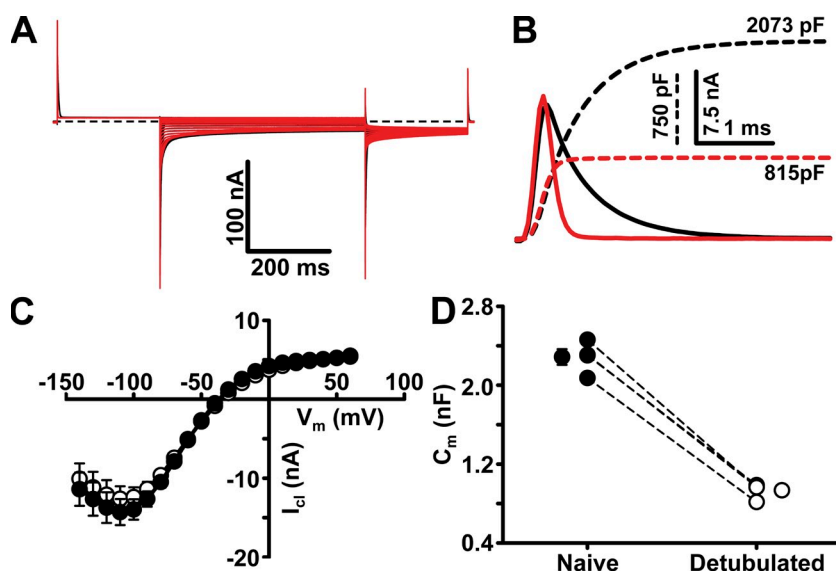

Figure 6. ClC-1 current is similar in FDB fibers from 4-mo-old mice before and after formamide detubulation in paired experiments, despite a significant reduction in membrane capacitance. (A) Families of 9-AC–sensitive ClC-1 currents recorded from a representative FDB fiber from a 4-mo-old mouse before (black) and after (red) formamide addition and withdrawal. (B) Capacitive currents elicited by a depolarization from +90 to +100 mV before (solid black line) and after (solid red line) formamide addition and withdrawal for the fiber shown in A. Total cell capacitance for this fiber was reduced from 2,073 to 815 pF after formamide addition and withdrawal. (C) Average voltage dependence of steady-state ClC-1 currents recorded from FDB fibers from 4-mo-old mice before (filled symbols) and after (open symbols) detubulation. (D) Average membrane capacitance was significantly reduced 59.2 ± 0.1% ($n = 4$) in FDB fibers from 4-mo-old mice after formamide addition and withdrawal. Data are presented as mean ± SEM ($n = 4$).

ClC-1 immunofluorescence exhibited a strictly sarcolemma staining pattern (Fig. 7 A, left), whereas DHPR immunostaining coincided with a parallel double row pattern of striation consistent with its selective T-tubule localization (Fig. 7 A, middle). The merged image of ClC-1 and DHPR immunostaining (Fig. 7 A, right) underscores the striking difference in the subcellular localization of these two proteins, consistent with previously published work in rat skeletal muscle (Papponen et al., 2005). However, these results do not preclude the potential concentration of ClC-1 channels at the T-tubule entry point or "neck." To more rigorously address this issue, normalized DHPR (T-tubule) and ClC-1 (sarcolemma) immunofluorescence intensities at the fiber periphery were plotted against longitudinal fiber distance. Analysis of these data revealed that the DHPR and ClC-1 signals peak with periodicities of 1 and 2 µm, but do so 90° out of phase from one another (Fig. 7, B and C), as shown by fast-Fourier transform analysis (Fig. 7 D).

Function and localization of expressed ClC-1 channels in mouse skeletal myotubes

Because the experiments in Fig. 7 relied on the use of an antibody directed against the C terminus of ClC-1, it is possible that the T-tubule system could contain a population of ClC-1 channels in which the C terminus is either truncated or where the C-terminal antibody epitope is masked. To address this issue, we generated a ClC-1 construct with GFP and FLAG tags on the N and C terminus, respectively (GFP-ClC-1-FLAG). To confirm that "tagging" the channel in this manner does not alter function, we measured macroscopic ClC-1 currents in whole cell

voltage clamp experiments after the expression of untagged and tagged ClC-1 channels in RYR1-null (dyspedic) skeletal myotubes, which serves as an excellent homologous ClC-1 expression system (Lueck et al., 2007b) because of the absence of endogenous ClC-1 activity in myotubes. GFP-ClC-1-FLAG–expressing myotubes exhibited macroscopic currents with all of the hallmarks of classical ClC-1 channel activity, including chloride selectivity (E_{rev} being close to E_{Cl}; Fig. 8 A), instantaneous and steady-state current–voltage relationships with characteristic inward rectification and "S"-shaped voltage dependence, respectively (Fig. 8 B), a weak voltage dependence to Po_{rel} (Fig. 8 C), and rapid and voltage-dependent channel deactivation kinetics (unpublished data). These results indicate that the introduced N- and C-terminal tags do not significantly alter ClC-1 channel function.

GFP-ClC-1-FLAG–expressing myotubes were fixed and immunofluorescently labeled with an antibody directed against the α_{1S} subunit of the DHPR. Consistent with previous reports, the skeletal muscle DHPR exhibited a discrete punctate appearance in myotubes (Fig. 8 E), which correlates with "peripheral couplings" between the SR and sarcolemma that represent locations of early T-tubule formation (Protasi et al., 1997). In the same cells, GFP-ClC-1-FLAG exhibited both uniform sarcolemma localization (Fig. 8 D, filled arrows) and intracellular aggregates (Fig. 8 D, open arrows), consistent with the incomplete processing and trafficking of some ClC-1 channels (Papponen et al., 2005). Merged images (Fig. 8 F) demonstrate the absence of DHPR and GFP-ClC-1-FLAG colocalization, indicating that ClC-1 is not preferentially targeted to peripheral couplings.
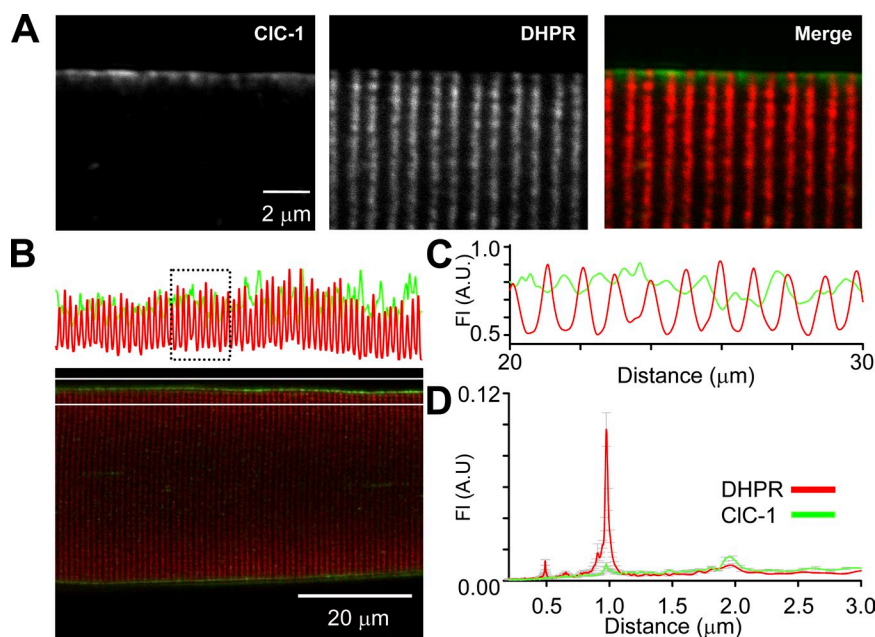
Figure 7. Native ClC-1 channels localize to the sarcolemma in FDB fibers from adult mice. (A) Immunofluorescence of native ClC-1 channels (left) and DHPRs (middle) in a representative FDB fiber from an adult mouse. The absence of ClC-1 and DHPR colocalization is highlighted by merging the two images (right). (B) The fluorescence intensity profile (top) from a confocal image of a representative FDB fiber from an adult mouse (bottom), showing regular periodicity of both ClC-1 (green) and DHPR (red) fluorescence signals. (C) Expanded view of the fluorescence intensity profile in the boxed region shown in B emphasizes that although the ClC-1 and DHPR signals share a similar regular periodicity, they are 90° out of phase. (D) The average (±SEM) results of fast-Fourier transformation analyses of fluorescence profiles from 26 experiments reveal that the ClC-1 and DHPR signals peak with a periodicity of 1 and 2 µm.

Adenoviral expression of GFP-ClC-1-FLAG channels in skeletal muscle of *HSA*LR mice

We next set out to determine the function and subcellular localization of expressed ClC-1 channels in fully differentiated adult skeletal muscle. *HSA*LR transgenic mice are a mouse model for myotonic dystrophy, as they exhibit hyperexcitable skeletal muscle (Mankodi et al., 2000) as a result of reduced expression of ClC-1. Owing to a defect in splicing regulation, the ClC-1 transcript in these mice contains a premature termination codon, and the level of functional ClC-1 channels is reduced by >70% (Lueck et al., 2007a,b). Therefore, we injected adeno-
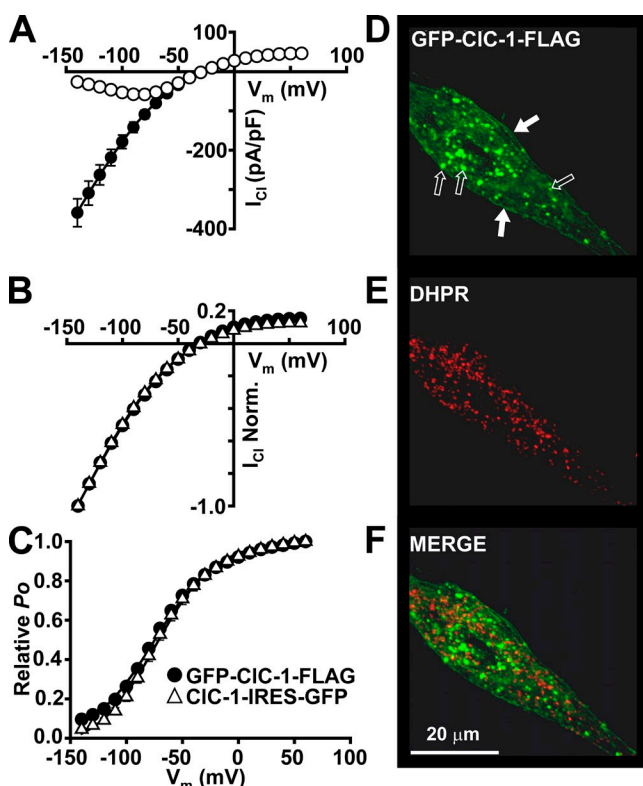
viruses encoding either GFP or GFP-ClC-1-FLAG into contralateral TA muscles of 2-d-old WT ($n = 6$) and *HSA*LR ($n = 14$) mouse pups. 3 wk after adenovirus injection, mice were assessed for myotonia using EMG analysis, and TA muscles were subsequently removed, sectioned, and evaluated for GFP fluorescence.

Analysis of transverse cryosections of TA muscles revealed that adenoviral injection resulted in expression of both GFP-ClC-1-FLAG and GFP with ∼70% transduction efficiency in the region of injection (Fig. 9 A). Although GFP fluorescence displayed a diffuse myoplasmic expression pattern (Fig. 9 A, left), GFP-ClC-1-FLAG exhibited both robust sarcolemmal expression and a low level of intracellular localization in some fibers (Fig. 9 A, right). To determine if the intracellular localization of GFP-ClC-1-FLAG channels was within the
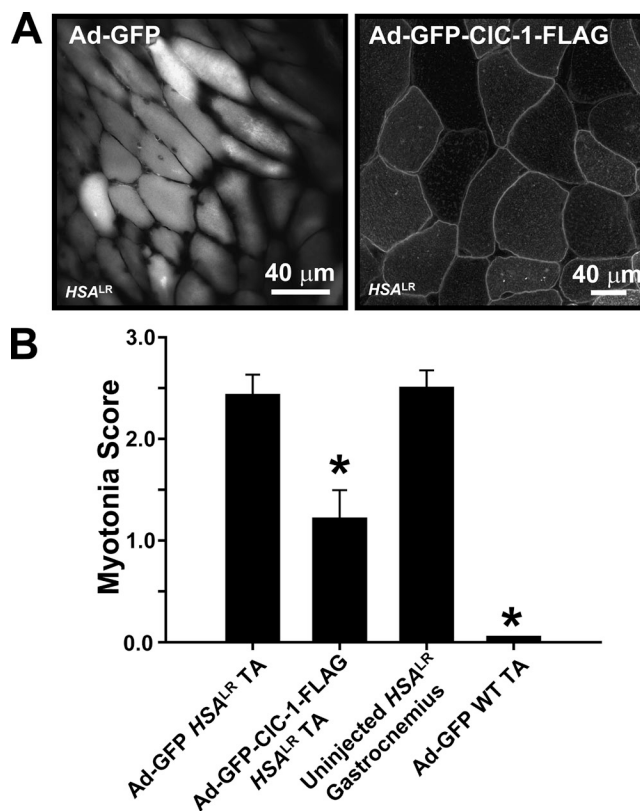

Figure 8. GFP-ClC-1-FLAG channels expressed in myotubes function normally and traffic to the sarcolemma, but not to DHPR-containing peripheral junctions. (A) GFP-ClC-1-FLAG channels expressed in dyspedic myotubes exhibit normal voltage dependence of steady-state (open circles) and instantaneous (filled circles) current. (B) Superimposed and normalized (to current at −140 mV) instantaneous current–voltage relationships obtained from myotubes expressing either GFP-ClC-1-FLAG (filled circles) or ClC-1 (open triangles). (C) Average relative *Po-V* curves obtained from tail currents elicited at −100 mV for myotubes expressing GFP-ClC-1-FLAG (filled circles) or ClC-1 (open triangles). Smooth curves through each dataset were generated using a modified Boltzmann equation (Eq. 3). Data in A–C are presented as mean ± SEM of eight and seven experiments for GFP-ClC-1-FLAG– and ClC-1-IRES-GFP–expressing myotubes, respectively. GFP-ClC-1-FLAG fluorescence (D) does not colocalize with DHPR immunofluorescence (E), as emphasized in the merged image (F). In D, black arrows show intracellular aggregates, and white arrows show areas of uniform sarcolemmal expression. DHPRs reside in puncta representing peripheral junctions between the SR and sarcolemma.

Figure 9. Adenoviral-mediated expression of GFP-ClC-1-FLAG significantly reverses myotonia in TA muscle of *HSA*LR mice. (A) GFP fluorescence of cross sections of *HSA*LR TA muscle showing distribution of cytosolic GFP (left) and GFP-ClC-1-FLAG (right) 3 wk after injection. Note that the images represent regions of transduction at the site of injection and are not representative of the total muscle body. (B) Myotonia score (see Materials and methods) was significantly reduced in the TA muscle of *HSA*LR mice after adenoviral-mediated expression of GFP-ClC-1-FLAG compared with contralateral TA muscle expressing cytoplasmic GFP. Non-transduced gastrocnemius muscle from *HSA*LR mice served as an untreated positive control. Data are presented as mean ± SEM (6 and 14 experiments for WT and *HSA*LR mice, respectively). A one-way ANOVA with Tukey's post-hoc test was used for group comparisons. *, $P \leq 0.01$.

T-tubule membrane, RYR1 was immunolabeled as a marker of the sarcotubular system (Fig. 10). Under closer inspection, it was clear that a significant population of ClC-1 channels resided at the sarcolemma (Fig. 10 A), consistent with previous results for the native channel using a ClC-1 channel C-terminal antibody (Gurnett et al., 1995; Mankodi et al., 2002; Wheeler et al., 2007, 2009). RYR1 staining in transverse sections (Fig. 10 B) exhibited a reticulated pattern similar to that shown previously for the DHPR (Ohlendieck et al., 1991; Takekura and Franzini-Armstrong, 1999). Merged images of GFP-ClC-1-FLAG and RYR1 fluorescence revealed the absence of significant intracellular colocalization (Fig. 10 C), consistent with the absence of significant T-tubular localization of the expressed channel. Analysis of longitudinal sections also confirmed clear GFP-ClC-1-FLAG sarcolemma localization and the absence of a significant transverse fluorescence (Fig. 10 D). Conversely, RYR1 immunofluorescence in longitudinal sections exhibited robust double transverse rows (Fig. 10 E), consistent with the known triadic localization of RYR1 (Takekura and Franzini-Armstrong, 1999). These results indicate that the expressed GFP-ClC-1-FLAG channels localized primarily to the skeletal muscle sarcolemma, although low level expression within the T-tubule system cannot be excluded.

EMG analysis revealed that prominent myotonic discharges were significantly reduced 3 wk after TA muscles of HSA^{LR} mice were injected with adenovirus-encoding GFP-ClC-1-FLAG channels, but not a control GFP adenovirus (Fig. 9 B). WT TA muscles exhibited no myotonic discharges after the injection of adenovirus for either GFP (Fig. 9 B) or GFP-ClC-1-FLAG (unpublished data). Importantly, electrical activity as a result of needle insertion was not reduced for any condition, indicating that muscles were not damaged, electrically "silent," or unable to elicit action potentials. Collectively, the results presented in Figs. 9 and 10 indicate that the GFP-ClC-1-FLAG adenovirus injections resulted in robust ClC-1 expression in the sarcolemma and partial functional rescue of the enhanced skeletal muscle excitability, which is characteristic of HSA^{LR} mice.

DISCUSSION

The relative subcellular distribution of chloride channels between the sarcolemma and T-tubule membrane in skeletal muscle has long been debated. We directly addressed this issue using three independent approaches: macroscopic measurements of ClC-1 channel activity in FDB fibers before and after detubulation, simultaneous, high resolution subcellular immunodetection of endogenous ClC-1 and DHPR proteins, and rescue of myotonia susceptibility in HSA^{LR} mice with a GFP-ClC-1-FLAG adenovirus. Important contributions of this study include: (a) demonstration that chloride channel current amplitude and properties (i.e., voltage dependence and kinetics) in FDB fibers from young and adult mice are unaffected by a marked loss in T-tubule membrane after formamide-induced detubulation (Figs. 1–6); (b) identification of endogenous ClC-1 immunoreactivity concentrated within regions of the sarcolemma located between sites of T-tubule invagination (Fig. 7); and (c) partial rescue of myotonia in TA of HSA^{LR} mice after adenoviral-mediated delivery of ClC-1 channels in the muscle sarcolemma (Figs. 8–10). Collectively, these results indicate that functional ClC-1 channels in mouse
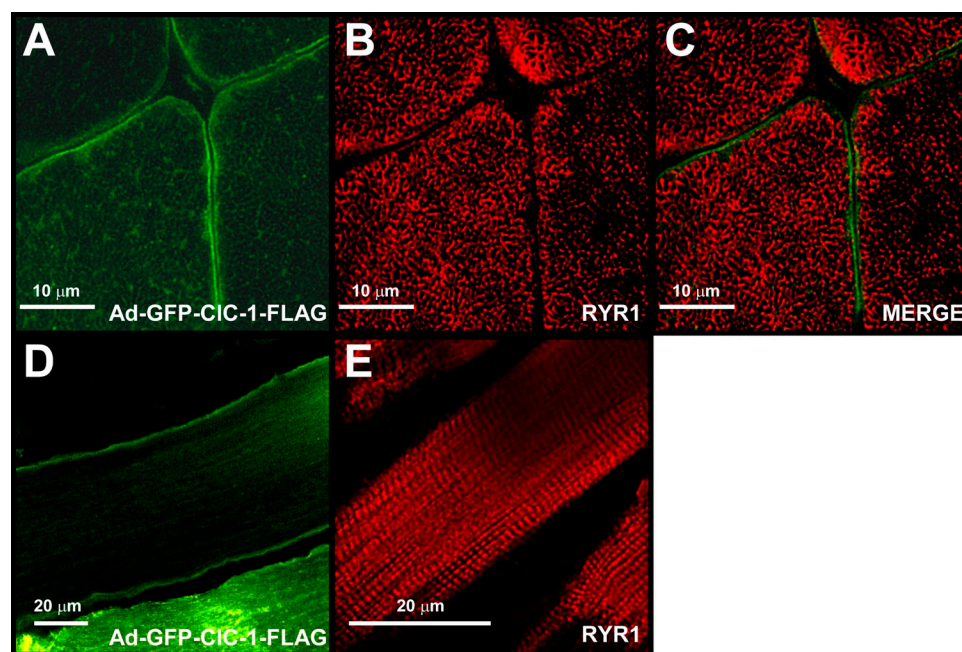
Figure 10. GFP-ClC-1-FLAG fluorescence does not localize to triads after expression in adult skeletal muscle. (A) GFP fluorescence of a representative transverse section of TA muscle from an HSA^{LR} mouse 3 wk after injection of GFP-ClC-1-FLAG adenovirus. (B) RYR1 immunofluorescence of the same field as that shown in A. (C) Merged image of the images shown in A and B. (D and E) GFP fluorescence (D) and RYR1 immunofluorescence (E) images from representative longitudinal sections of TA muscle from HSA^{LR} mice 3 wk after injection of GFP-ClC-1-FLAG adenovirus.

skeletal muscle are located within the sarcolemma and not the T-tubule system.

Subcellular localization of endogenous ClC-1 channels in mouse skeletal muscle

Previous studies used membrane fractionation and immunofluorescence approaches to conclude that ClC-1 protein localizes primarily to the sarcolemma (Gurnett et al., 1995; Mankodi et al., 2002; Wheeler et al., 2007, 2009). However, physiological membrane potential (Dulhunty, 1979), chloride conductance (Palade and Barchi, 1977), and contractile measurements (Coonan and Lamb, 1998; Dutka et al., 2008) in skeletal muscle have suggested that functional ClC-1 channels are located largely in the T-tubule membrane system. Using the whole cell patch clamp technique, we provide the first direct characterization of the magnitude and biophysical properties of endogenous ClC-1 channel activity in mouse skeletal muscle fibers before and after formamide-induced detubulation. In our experiments, ClC-1 currents were isolated by eliminating sodium (0 extracellular sodium), potassium (substitution of extracellular and intracellular potassium with TEA and cesium, respectively), and calcium (250 µM cadmium) currents. Under these conditions, 0.5 mM 9-AC blocked 98% of all chloride conductance, arguing against a significant contribution of 9-AC–insensitive chloride channels in our experiments. Additionally, calcium-activated chloride channels would likely be inhibited/blocked under our recording conditions, as experiments were performed in the presence of 10 mM of intracellular EGTA. Furthermore, all recorded chloride currents exhibited inward rectification, even at very positive potentials, and thus, did not appear to contain a component as a result of outwardly rectifying calcium-activated chloride channels (Schroeder et al., 2008; Yang et al., 2008).

Several methodologies have been used previously to discriminate between total and sarcolemmal chloride conductance in skeletal muscle. The most common approach has been to use glycerol-induced osmotic shock to detubulate muscle fibers (Eisenberg and Gage, 1969). However, the effects of glycerol-induced osmotic shock on skeletal muscle chloride conductance are inconsistent, with differing results obtained between amphibian and mammalian skeletal muscle, as well as between separate studies using the same species (for review see Bretag, 1987). Our attempts to measure ClC-1 channel function in FDB fibers after the disruption of T-tubules with glycerol shock were unsuccessful because the treatment resulted in irreversible damage to the cell membrane, as reflected in obtaining only low resistance seals in whole cell patch clamp experiments. These results are consistent with previous findings that glycerol shock results in membrane depolarization (Dulhunty, 1979; Davey et al., 1980) and is more effective in detubulating

amphibian skeletal muscle compared with either mammalian cardiac (Niemeyer and Forssmann, 1971) or skeletal muscle (Davey et al., 1980). On the other hand, we routinely obtained high resistance seals and voltage clamp recordings after formamide-induced detubulation, which is highly effective in detubulating frog skeletal muscle (del Castillo and Escalona de Motta, 1978), as well as mammalian cardiac (Kawai et al., 1999; Brette et al., 2002), smooth (Córdoba et al., 1968), and skeletal (Bournaud and Mallart, 1987) muscle. Using this approach, detubulation did not significantly alter ClC-1 chloride current magnitude, voltage dependence, or gating in FDB fibers from both young (Figs. 1–5) and adult (Fig. 6) mice, despite a marked reduction in T-tubule membrane content. These results are consistent with the majority of functional ClC-1 channels in mouse FDB fibers residing within the sarcolemma.

We validated the degree of formamide-induced detubulation using both fluorescence and electrophysiological approaches. First, transverse but not sarcolemmal di-8-ANEPPS fluorescence was essentially abolished when fibers were stained after formamide addition and withdrawal (Fig. 1 A). Second, formamide treatment caused ∼40% reduction of total membrane capacitance in fibers from 15–16-d-old mice (Figs. 2, C and D, and 4 B) and a 61% reduction in fibers from 4-mo-old mice (Fig. 6 D). The difference in fractional reduction in membrane capacitance between fibers obtained from young and adult mice most likely reflects the fact that the T-tubule system increases fivefold (Luff and Atwood, 1971) and does not reach full maturity until several weeks after birth (Beam and Knudson, 1988b; Franzini-Armstrong, 1991). Previous estimates suggest that after taking into account caveolae, the T-tubule system comprises ∼71% of the total cell capacitance in adult mammalian skeletal muscle (Dulhunty et al., 1984). Given these estimates, the formamide treatment protocol used in this study resulted in an ∼85% loss of T-tubule membrane content ($0.61/0.71 = 0.85$) in adult mice, with the remaining 15% presumably a result of incomplete detubulation and retention of initial T-tubule segments or necks (Fig. 1 A, right, arrows).

We initially considered irreversible direct or secondary effects of formamide on ClC-1 channels as a potential concern in the detubulation experiments conducted in this study. However, an irreversible effect of formamide on ClC-1 channel function is unlikely because the magnitude and biophysical properties (i.e., deactivation kinetics, voltage dependence, and rectification) of the 9-AC–sensitive current were unaltered after the addition and removal of formamide (Figs. 1–6). To our knowledge, direct effects of glycerol on ClC-1 function have not been similarly assessed, and thus, may contribute to some of the differences observed in prior studies. The absence of altered ClC-1 channel deactivation kinetics after formamide-induced detubulation (Figs. 3 and 5)

has several important implications. First, these findings validate adequate space clamp uniformity even in naive fibers because ClC-1 channel gating was unaffected by loss of a significant fraction of cell capacitance originating from the T-tubule compartment. Second, previous studies demonstrated that ClC-1 gating is strongly influenced by chloride concentration (Rychkov et al., 1996, 1997; Accardi and Pusch, 2000; Chen and Chen, 2001), pH (Rychkov et al., 1996, 1997; Accardi and Pusch, 2000; Chen and Chen, 2001; Bennetts et al., 2007), nitric oxide (Lin et al., 2008), and with some controversy, the binding of adenosine derivatives (Bennetts et al., 2005, 2007; Tseng et al., 2007; Zhang et al., 2008; Zifarelli and Pusch, 2008). Although we did not directly test if these factors modulate native ClC-1 channel activity in FDB fibers, our findings suggest that detubulation by formamide addition and withdrawal does not markedly perturb basal modulatory influences of these factors on ClC-1 gating.

Our high resolution confocal measurements of DHPR/ClC-1 immunofluorescence in single intact FDB fibers indicate that ClC-1 is not concentrated at regions of T-tubule invagination (Fig. 7). In addition, these results suggest that our observation that ClC-1 channel activity is unaffected by formamide-induced detubulation is not a result of a rapid redistribution of channels from the T-tubule system to the sarcolemma during whole cell patch clamp dialysis. However, because the results in Fig. 7 were obtained using an antibody directed to the C terminus of the ClC-1 protein, it is possible that a subpopulation of truncated ClC-1 channels resides within this junctional region and contributes to a fraction of the measured ClC-1 channel activity. Indeed, using di-8-ANEPPS to visualize membrane accessible to the extracellular solution, we found that initial segments of presumed sites of T-tubule invagination were retained after formamide-induced detubulation (Fig. 1 A). Thus, we cannot rule out a possible contribution of truncated ClC-1 channels within the initial sites of T-tubule invagination retained after detubulation to the total 9-AC–sensitive ClC-1 conductance in our experiments. Nevertheless, our demonstration of the vast majority of native ClC-1 immunofluorescence residing within regions of the sarcolemma not associated with T-tubule invaginations indicates that sarcolemma ClC-1 channels account for the majority of ClC-1 function in intact muscle fibers.

Rescue of enhanced muscle excitability in HSA^{LR} via ClC-1 gene transfer

We previously reported that myotonia in two different mouse models of DM1 results from a dramatic reduction in skeletal muscle ClC-1 channel function (Lueck et al., 2007b). Injection of morpholino antisense oligonucleotides targeted to ClC-1 premRNA rescued ClC-1 channel function and significantly reduced myotonia in

HSA^{LR} mice (Wheeler et al., 2007). Moreover, injection of morpholino antisense oligonucleotides that bind to CUG repeat expansion RNA and block its interaction with muscleblind-like 1 also restored ClC-1 channel function and reduced myotonia in HSA^{LR} mice (Wheeler et al., 2009). Here, we reduced myotonia in TA muscles of HSA^{LR} mice by directly increasing ClC-1 channel expression through adenoviral-mediated gene transfer (Fig. 9 B). The fact that myotonia was only partially reduced rather than abolished most likely reflects the fact that a single injection of GFP-ClC-1-FLAG adenovirus resulted in partial transduction and uneven/patchy expression of the injected muscle. Nevertheless, these results provide evidence that myotonia rescue in DM1 can result in exogenous expression of functional ClC-1 channels alone. Although our studies provide no indication of deleterious effects of exogenous ClC-1 expression, it is nonetheless a concern because ClC-1 overexpression could potentially compromise normal muscle excitability (DiFranco et al., 2009). However, our results suggest that proper delivery of muscle ClC-1 channels through adenoviral gene therapy could provide a viable approach for alleviating myotonia in DM1 and myotonia congenita.

Previous studies using a C-terminal directed antibody identified endogenous ClC-1 channels exclusively in the sarcolemma (Gurnett et al., 1995; Mankodi et al., 2002; Papponen et al., 2005; Wheeler et al., 2007, 2009). However, as discussed above, the T-tubule system could contain a population of ClC-1 channels in which the C terminus is truncated or where the C-terminal antibody epitope is masked as a result of altered ClC-1 folding, posttranslational modification, protein binding, or premRNA splicing. In this study, we used an N-terminal GFP-tagged ClC-1 construct to assess ClC-1 localization in a manner independent of the C terminus. We found that the addition of an N-terminal GFP tag does not alter ClC-1 function based on the normal biophysical properties of the tagged channel after homologous expression in myotubes (Fig. 8, A–C) and a significant reduction in muscle hyperexcitability in the TA of HSA^{LR} mice after adenoviral-mediated transduction (Fig. 9 B). Importantly, we found that expression of GFP-ClC-1-FLAG in both skeletal myotubes and fully differentiated skeletal muscle resulted in prominent sarcolemma GFP fluorescence in the absence of colocalization of either the DHPR or RYR1, well-established markers of the sarcotubular system. As an alternate approach, we determined the subcellular localization of exogenously expressed ClC-1 channels containing a Btx-binding site inserted in an extracellular loop (Btx-ClC-1; Fig. S1 A). The Btx-binding site insertion did not alter ClC-1 function (Fig. S1, C–E), and the incubation of expressing myotubes (Fig. S1 B) and FDB fibers (Fig. S1 F, right) with Alexa 594–conjugated α-Btx resulted in selective staining of the sarcolemma. In these experiments, the

combined use of an extracellular tag and membrane-impermeable fluorescent label enabled clear demonstration that Btx-ClC-1 channels were fully processed and trafficked to the sarcolemma and not the T-tubule system. Control experiments using a nonspecific membrane protein (Btx-ΔRAMP1) expressed in FDB fibers confirmed adequate Alexa 594–conjugated α-Btx accessibility within the T-tubule system (Fig. S1 F, left). The preferential localization of both endogenous (Gurnett et al., 1995; Mankodi et al., 2002; Papponen et al., 2005; Wheeler et al., 2007, 2009) and exogenously expressed (Fig. 9 A) ClC-1 channels within the sarcolemma in cross sections of intact muscles indicates that our finding that ClC-1 channel activity in isolated fibers arises from sarcolemma channels is unlikely to be a result of a redistribution of channels that occurs during single fiber isolation. Although we cannot exclude the possible effects of the GFP and Btx tags on normal ClC-1 trafficking, or that a small fraction of channels in the T-tubule membrane escaped detection, these results indicate that the majority of the expressed ClC-1 channels localize to the sarcolemma, consistent with previous studies showing sarcolemmal-restricted localization of N-terminal myc-tagged ClC-1 channels expressed in cultured mouse FDB fibers (Papponen et al., 2005).

G_{Cl} stabilization of skeletal muscle excitability by remote control

Each skeletal muscle action potential results in a small increase in potassium ($\sim$0.3 mM) within the diffusion-limited space of the T-tubule lumen (Adrian and Marshall, 1976; Cannon et al., 1993). Thus, during repetitive muscle activity, T-tubule potassium accumulation is compounded and can result in significant membrane depolarization, enhanced muscle excitability, and eventually myotonia if not counteracted by a large, stabilizing ClC-1 chloride conductance (Adrian and Bryant, 1974; Cannon et al., 1993). Consistent with this, DiFranco et al. (2005) demonstrated that immediately after brief tetanic stimulation of mouse FDB fibers (200 Hz and 100 ms), repolarization is less complete within the T-tubule system and is therefore depolarized compared with the sarcolemma. Because potassium accumulation and depolarization of E_K during repetitive stimulation are greater within the T-tubule, it is reasonable to assume the stabilizing chloride conductance would also likely originate within the T-tubule system. However, results presented here using multiple complementary approaches indicate that the vast majority of ClC-1 chloride conductance in mouse FDB fibers resides within the sarcolemma.

How could the activity of sarcolemmal-restricted ClC-1 channels stabilize skeletal muscle excitability in the face of the depolarizing effects of the progressive potassium accumulation that occurs within the T-tubule system? As one possibility, we propose a "remote control" model

for G_{Cl} stabilization of membrane excitability, whereby ClC-1 channels localized to sites distant from that of potassium accumulation is advantageous by ensuring that G_{Cl} remains unaltered by the depolarizing effects of potassium accumulation in the T-tubule system. Because chloride permeability comprises up to $\sim$80% of the total resting membrane conductance in mammalian skeletal muscle (Hutter and Padsha, 1959; Aromataris and Rychkov, 2006), G_{Cl} provides a powerful electrical shunt, or safeguard, against transient changes in V_m. However, the ability of G_{Cl} within the T-tubule system to counteract increased excitability as a result of potassium accumulation will ultimately be limited by the passive movement of chloride ions over time as E_{Cl} closely follows E_K (Adrian, 1961). Conversely, localization of ClC-1 channels (and thus G_{Cl}) within a membrane compartment where E_K does not change during repetitive stimulation (i.e., the sarcolemma) would ensure that E_{Cl} remains negative to the depolarized E_K (and V_m) of the T-tubule system during potassium accumulation. In this scenario, sarcolemmal G_{Cl} would continue to counteract depolarization within the T-tubule system, provided that G_{Cl} is large enough and adequate electrical coupling exists between the two membrane compartments. Indeed, elegant voltage and current clamp studies paired with optical di-8-ANEPPS measurements of the T-tubule membrane potential provide strong evidence for efficient electrical coupling between membrane potential changes in the sarcolemma and T-tubule systems in mammalian skeletal muscle fibers (DiFranco et al., 2005; Woods et al., 2005). Interestingly, this is not the case in amphibian skeletal muscle, where a significant delay is observed between voltage changes in the sarcolemma and T-tubule system (Heiny and Vergara, 1982; Heiny et al., 1983; Ashcroft et al., 1985; Kim and Vergara, 1998a,b). The electrical coupling between the sarcolemma and T-tubule system in mammalian muscle fibers may be more efficient than amphibian muscle fibers because they exhibit a significantly smaller: (a) access resistance between the T-tubule lumen and extracellular solution (Adrian and Peachey, 1973; Kim and Vergara, 1998b); (b) T-tubule luminal resistance (Adrian et al., 1969; Ashcroft et al., 1985; Kim and Vergara, 1998b); and (c) fiber diameter (Adrian et al., 1969; Kim and Vergara, 1998b). Thus, we propose that the combination of a maintained large G_{Cl} within the sarcolemma and efficient electrical coupling between the sarcolemmal and T-tubule membrane systems constitutes a remote control mechanism for G_{Cl}-mediated stabilization of mammalian skeletal muscle excitability after repetitive stimulation.

Concluding remarks

Previous studies have convincingly demonstrated that skeletal muscle ClC-1 channel function is required to maintain normal skeletal muscle excitability during

high frequency stimulation. Here, we provide strong evidence that the functionally relevant ClC-1 channel conductance resides within the sarcolemma of mouse skeletal muscle fibers. Although our experiments were designed to specifically assess ClC-1 channel activity, our results do not preclude possible contributions of other chloride channels (e.g., Ca^{2+}-activated chloride channels) to the total muscle chloride conductance. Moreover, these other chloride channels could potentially be located within the T-tubule system and contribute to stabilization of normal muscle excitability during high frequency stimulation.

REFERENCES

Accardi, A., and M. Pusch. 2000. Fast and slow gating relaxations in the muscle chloride channel CLC-1. *J. Gen. Physiol.* 116:433–444. doi:10.1085/jgp.116.3.433

Adrian, R.H. 1961. Internal chloride concentration and chloride efflux of frog muscle. *J. Physiol.* 156:623–632.

Adrian, R.H., and S.H. Bryant. 1974. On the repetitive discharge in myotonic muscle fibres. *J. Physiol.* 240:505–515.

Adrian, R.H., and M.W. Marshall. 1976. Action potentials reconstructed in normal and myotonic muscle fibres. *J. Physiol.* 258:125–143.

Adrian, R.H., and L.D. Peachey. 1973. Reconstruction of the action potential of frog sartorius muscle. *J. Physiol.* 235:103–131.

Adrian, R.H., L.L. Costantin, and L.D. Peachey. 1969. Radial spread of contraction in frog muscle fibres. *J. Physiol.* 204:231–257.

Allen, D.G., G.D. Lamb, and H. Westerblad. 2008. Skeletal muscle fatigue: cellular mechanisms. *Physiol. Rev.* 88:287–332. doi:10.1152/physrev.00015.2007

Almers, W. 1980. Potassium concentration changes in the transverse tubules of vertebrate skeletal muscle. *Fed. Proc.* 39:1527–1532.

Andersson-Cedergren, E. 1959. Ultrastructure of motor end plate and sarcoplasmic components of mouse skeletal muscle fiber as revealed by three-dimensional reconstructions from serial sections. *J. Ultrastruct. Res.* 2:5–191. doi:10.1016/S0889-1605(59)80002-1

Armstrong, C.M., and W.F. Gilly. 1992. Access resistance and space clamp problems associated with whole-cell patch clamping. *Methods Enzymol.* 207:100–122. doi:10.1016/0076-6879(92)07007-B0305-1870,1440-1681

Aromataris, E.C., and G.Y. Rychkov. 2006. ClC-1 chloride channel: matching its properties to a role in skeletal muscle. *Clin. Exp. Pharmacol. Physiol.* 33:1118–1123.

Ashcroft, F.M., J.A. Heiny, and J. Vergara. 1985. Inward rectification in the transverse tubular system of frog skeletal muscle studied with potentiometric dyes. *J. Physiol.* 359:269–291.

Beam, K.G., and C.M. Knudson. 1988a. Calcium currents in embryonic and neonatal mammalian skeletal muscle. *J. Gen. Physiol.* 91:781–798. doi:10.1085/jgp.91.6.781

Beam, K.G., and C.M. Knudson. 1988b. Effect of postnatal development on calcium currents and slow charge movement in mammalian skeletal muscle. *J. Gen. Physiol.* 91:799–815. doi:10.1085/jgp.91.6.799

Bennett, H.S., and K.R. Porter. 1953. An electron microscope study of sectioned breast muscle of the domestic fowl. *Am. J. Anat.* 93:61–105.

Bennetts, B., G.Y. Rychkov, H.L. Ng, C.J. Morton, D. Stapleton, M.W. Parker, and B.A. Cromer. 2005. Cytoplasmic ATP-sensing domains regulate gating of skeletal muscle ClC-1 chloride channels. *J. Biol. Chem.* 280:32452–32458. doi:10.1074/jbc.M502890200

Bennetts, B., M.W. Parker, and B.A. Cromer. 2007. Inhibition of skeletal muscle ClC-1 chloride channels by low intracellular pH and ATP. *J. Biol. Chem.* 282:32780–32791. doi:10.1074/jbc.M703259200

Bournaud, R., and A. Mallart. 1987. An electrophysiological study of skeletal muscle fibres in the 'muscular dysgenesis' mutation of the mouse. *Pflugers Arch.* 409:468–476. doi:10.1007/BF00583803

Bretag, A.H. 1987. Muscle chloride channels. *Physiol. Rev.* 67:618–724.

Brette, F., K. Komukai, and C.H. Orchard. 2002. Validation of formamide as a detubulation agent in isolated rat cardiac cells. *Am. J. Physiol. Heart Circ. Physiol.* 283:H1720–H1728.

Cannon, S.C., R.H. Brown Jr., and D.P. Corey. 1993. Theoretical reconstruction of myotonia and paralysis caused by incomplete inactivation of sodium channels. *Biophys. J.* 65:270–288. doi:10.1016/S0006-3495(93)81045-2

Chen, M.F., and T.Y. Chen. 2001. Different fast-gate regulation by external Cl− and H+ of the muscle-type ClC chloride channels. *J. Gen. Physiol.* 118:23–32.

Coonan, J.R., and G.D. Lamb. 1998. Effect of transverse-tubular chloride conductance on excitability in skinned skeletal muscle fibres of rat and toad. *J. Physiol.* 509:551–564.

Córdoba, F., S. Schoof, S. Vélez, and J. del Castillo. 1968. Inhibitory action of formamide on smooth muscle contraction. *Life Sci.* 7:897–903. doi:10.1016/0024-3205(68)90094-5

Costantin, L.L. 1976. Contractile activation in skeletal muscle. *Prog. Biophys. Mol. Biol.* 29:197–224. doi:10.1016/0079-6107(76)90023-7

Davey, D.F., A.F. Dulhunty, and D. Fatkin. 1980. Glycerol treatment in mammalian skeletal muscle. *J. Membr. Biol.* 53:223–233. doi:10.1007/BF01868828

del Castillo, J.G., and G. Escalona de Motta. 1978. A new method for excitation-contraction uncoupling in frog skeletal muscle. *J. Cell Biol.* 78:782–784.

DiFranco, M., J. Capote, and J.L. Vergara. 2005. Optical imaging and functional characterization of the transverse tubular system of mammalian muscle fibers using the potentiometric indicator di-8-ANEPPS. *J. Membr. Biol.* 208:141–153. doi:10.1007/s00232-005-0825-9

DiFranco, M., J. Capote, M. Quiñonez, and J.L. Vergara. 2007. Voltage-dependent dynamic FRET signals from the transverse tubules in mammalian skeletal muscle fibers. *J. Gen. Physiol.* 130:581–600.

DiFranco, M., M. Quinonez, J. Capote, and J.L. Vergara. 2009. DNA transfection of mammalian skeletal muscles using in vivo electroporation. *J. Vis. Exp.* 32:1520.doi.10.3791/1520

Dirksen, R.T. 2002. Bi-directional coupling between dihydropyridine receptors and ryanodine receptors. *Front. Biosci.* 7:d659–d670. doi:10.2741/dirksen

Dulhunty, A.F. 1979. Distribution of potassium and chloride permeability over the surface and T-tubule membranes of mammalian skeletal muscle. *J. Membr. Biol.* 45:293–310.

Dulhunty, A.F. 2006. Excitation-contraction coupling from the 1950s into the new millennium. *Clin. Exp. Pharmacol. Physiol.* 33:763–772. doi:10.1111/j.1440-1681.2006.04441.x

Dulhunty, A.F., G. Carter, and C. Hinrichsen. 1984. The membrane capacity of mammalian skeletal muscle fibres. *J. Muscle Res. Cell Motil.* 5:315–332.

Dutka, T.L., R.M. Murphy, D.G. Stephenson, and G.D. Lamb. 2008. Chloride conductance in the transverse tubular system of rat skeletal muscle fibres: importance in excitation-contraction coupling and fatigue. *J. Physiol.* 586:875–887. doi:10.1113/jphysiol.2007.144667

Edwards, G.A., and H. Ruska. 1955. The function and metabolism of certain insect muscles in relation to their structure. *Q. J. Microsc. Sci.* 96:151–159.

Eisenberg, R.S., and P.W. Gage. 1969. Ionic conductances of the surface and transverse tubular membranes of frog sartorius fibers. *J. Gen. Physiol.* 53:279–297. doi:10.1085/jgp.53.3.279

Franzini-Armstrong, C. 1991. Simultaneous maturation of transverse tubules and sarcoplasmic reticulum during muscle differentiation in the mouse. *Dev. Biol.* 146:353–363.

Fukuda, J., and K. Kawa. 1977. Permeation of manganese, cadmium, zinc, and beryllium through calcium channels of an insect muscle membrane. *Science.* 196:309–311. doi:10.1126/science.847472

Furman, R.E., and R.L. Barchi. 1977. The mechanism of myotonia induced by aromatic carboxylic acids. *Neurology.* 4:378.

Gurnett, C.A., S.D. Kahl, R.D. Anderson, and K.P. Campbell. 1995. Absence of the skeletal muscle sarcolemma chloride channel ClC-1 in myotonic mice. *J. Biol. Chem.* 270:9035–9038. doi:10.1074/jbc.270.16.9035

Hamill, O.P., A. Marty, E. Neher, B. Sakmann, and F.J. Sigworth. 1981. Improved patch-clamp techniques for high-resolution current recording from cells and cell-free membrane patches. *Pflugers Arch.* 391:85–100.

Heiny, J.A., and J. Vergara. 1982. Optical signals from surface and T system membranes in skeletal muscle fibers. Experiments with the potentiometric dye NK2367. *J. Gen. Physiol.* 80:203–230. doi:10.1085/jgp.80.2.203

Heiny, J.A., F.M. Ashcroft, and J. Vergara. 1983. T-system optical signals associated with inward rectification in skeletal muscle. *Nature.* 301:164–166.

Hodgkin, A.L., and P. Horowicz. 1959. The influence of potassium and chloride ions on the membrane potential of single muscle fibres. *J. Physiol.* 148:127–160.

Hodgkin, A.L., and P. Horowicz. 1960. The effect of sudden changes in ionic concentrations on the membrane potential of single muscle fibres. *J. Physiol.* 153:370–385.

Hutter, O.F., and S.M. Padsha. 1959. Effect of nitrate and other anions on the membrane resistance of frog skeletal muscle. *J. Physiol.* 146:117–132.

Huxley, A.F., and R.E. Taylor. 1958. Local activation of striated muscle fibres. *J. Physiol.* 144:426–441.

Kawai, M., M. Hussain, and C.H. Orchard. 1999. Excitation-contraction coupling in rat ventricular myocytes after formamide-induced detubulation. *Am. J. Physiol.* 277:H603–H609.

Kim, A.M., and J.L. Vergara. 1998a. Fast voltage gating of Ca^{2+} release in frog skeletal muscle revealed by supercharging pulses. *J. Physiol.* 511:509–518. doi:10.1111/j.1469-7793.1998.509bh.x

Kim, A.M., and J.L. Vergara. 1998b. Supercharging accelerates T-tubule membrane potential changes in voltage clamped frog skeletal muscle fibers. *Biophys. J.* 75:2098–2116. doi:10.1016/S0006-3495(98)77652-0

Kirsch, G.E., R.A. Nichols, and S. Nakajima. 1977. Delayed rectification in the transverse tubules: origin of the late after-potential in frog skeletal muscle. *J. Gen. Physiol.* 70:1–21. doi:10.1085/jgp.70.1.1

Leung, A.T., T. Imagawa, B. Block, C. Franzini-Armstrong, and K.P. Campbell. 1988. Biochemical and ultrastructural characterization of the 1,4-dihydropyridine receptor from rabbit skeletal muscle. Evidence for a 52,000 Da subunit. *J. Biol. Chem.* 263:994–1001.

Lin, M.J., R.Y. Huang, H. Pan, and K.M. Hsiao. 2008. Functional studies of the effect of NO donor on human CLCN1 polymorphism/mutants expressed in Xenopus laevis oocytes. *Biochem. Biophys. Res. Commun.* 365:724–728.

Lueck, J.D., C. Lungu, A. Mankodi, R.J. Osborne, S.L. Welle, R.T. Dirksen, and C.A. Thornton. 2007a. Chloride channelopathy in myotonic dystrophy resulting from loss of posttranscriptional regulation for CLCN1. *Am. J. Physiol. Cell Physiol.* 292:C1291–C1297. doi:10.1152/ajpcell.00336.2006

Lueck, J.D., A. Mankodi, M.S. Swanson, C.A. Thornton, and R.T. Dirksen. 2007b. Muscle chloride channel dysfunction in two mouse models of myotonic dystrophy. *J. Gen. Physiol.* 129:79–94. doi:10.1085/jgp.200609635

Luff, A.R., and H.L. Atwood. 1971. Changes in the sarcoplasmic reticulum and transverse tubular system of fast and slow skeletal muscles of the mouse during postnatal development. *J. Cell Biol.* 51:369–383. doi:10.1083/jcb.51.2.369

Mankodi, A., E. Logigian, L. Callahan, C. McClain, R. White, D. Henderson, M. Krym, and C.A. Thornton. 2000. Myotonic dystrophy in transgenic mice expressing an expanded CUG repeat. *Science.* 289:1769–1773.

Mankodi, A., M.P. Takahashi, H. Jiang, C.L. Beck, W.J. Bowers, R.T. Moxley, S.C. Cannon, and C.A. Thornton. 2002. Expanded CUG repeats trigger aberrant splicing of ClC-1 chloride channel pre-mRNA and hyperexcitability of skeletal muscle in myotonic dystrophy. *Mol. Cell.* 10:35–44.

Murphy, R.M., J.P. Mollica, and G.D. Lamb. 2009. Plasma membrane removal in rat skeletal muscle fibers reveals caveolin-3 hot-spots at the necks of transverse tubules. *Exp. Cell Res.* 315:1015–1028. doi:10.1016/j.yexcr.2008.11.022

Nakai, J., R.T. Dirksen, H.T. Nguyen, I.N. Pessah, K.G. Beam, and P.D. Allen. 1996. Enhanced dihydropyridine receptor channel activity in the presence of ryanodine receptor. *Nature.* 380:72–75. doi:10.1038/380072a0

Neelands, T.R., P.S. Herson, D. Jacobson, J.P. Adelman, and J. Maylie. 2001. Small-conductance calcium-activated potassium currents in mouse hyperexcitable denervated skeletal muscle. *J. Physiol.* 536:397–407. doi:10.1111/j.1469-7793.2001.0397c.xd

Niemeyer, G., and W.G. Forssmann. 1971. Comparison of glycerol treatment in frog skeletal muscle and mammalian heart. An electrophysiological and morphological study. *J. Cell Biol.* 50:288–299.

Ohlendieck, K.J., J.M. Ervasti, J.B. Snook, and K.P. Campbell. 1991. Dystrophin-glycoprotein complex is highly enriched in isolated skeletal muscle sarcolemma. *J. Cell Biol.* 112:135–148. doi:10.1083/jcb.112.1.135

Palade, P.T., and R.L. Barchi. 1977. Characteristics of the chloride conductance in muscle fibers of the rat diaphragm. *J. Gen. Physiol.* 69:325–342. doi:10.1085/jgp.69.3.325

Papponen, H., T. Kaisto, V.V. Myllylä, R. Myllylä, and K. Metsikkö. 2005. Regulated sarcolemmal localization of the muscle-specific ClC-1 chloride channel. *Exp. Neurol.* 191:163–173. doi:10.1016/j.expneurol.2004.07.018

Porter, K.R., and G.E. Palade. 1957. Studies on the endoplasmic reticulum. III. Its form and distribution in striated muscle cells. *J. Biophys. Biochem. Cytol.* 3:269–300.

Protasi, F., C. Franzini-Armstrong, and B.E. Flucher. 1997. Coordinated incorporation of skeletal muscle dihydropyridine

receptors and ryanodine receptors in peripheral couplings of BC3H1 cells. *J. Cell Biol.* 137:859–870.

Pusch, M. 2002. Myotonia caused by mutations in the muscle chloride channel gene CLCN1. *Hum. Mutat.* 19:423–434. doi:10.1002/humu.10063

Rychkov, G.Y., M. Pusch, D.S. Astill, M.L. Roberts, T.J. Jentsch, and A.H. Bretag. 1996. Concentration and pH dependence of skeletal muscle chloride channel ClC-1. *J. Physiol.* 497:423–435.

Rychkov, G.Y., D.S. Astill, B. Bennetts, B.P. Hughes, A.H. Bretag, and M.L. Roberts. 1997. pH-dependent interactions of Cd2+ and a carboxylate blocker with the rat C1C-1 chloride channel and its R304E mutant in the Sf-9 insect cell line. *J. Physiol.* 501:355–362. doi:10.1111/j.1469-7793.1997.355bn.x

Schroeder, B.C., T. Cheng, Y.N. Jan, and L.Y. Jan. 2008. Expression cloning of TMEM16A as a calcium-activated chloride channel subunit. *Cell.* 134:1019–1029.

Takekura, H., and C. Franzini-Armstrong. 1999. Correct targeting of dihydropyridine receptors and triadin in dyspedic mouse skeletal muscle in vivo. *Dev. Dyn.* 214:372–380.

Tseng, P.Y., B. Bennetts, and T.Y. Chen. 2007. Cytoplasmic ATP inhibition of CLC-1 is enhanced by low pH. *J. Gen. Physiol.* 130:217–221. doi:10.1085/jgp.200709817

Wheeler, T.M., J.D. Lueck, M.S. Swanson, R.T. Dirksen, and C.A. Thornton. 2007. Correction of ClC-1 splicing eliminates chloride channelopathy and myotonia in mouse models of myotonic dystrophy. *J. Clin. Invest.* 117:3952–3957.

Wheeler, T.M., K. Sobczak, J.D. Lueck, R.J. Osborne, X. Lin, R.T. Dirksen, and C.A. Thornton. 2009. Reversal of RNA dominance by displacement of protein sequestered on triplet repeat RNA. *Science.* 325:336–339.

Woods, C.E., D. Novo, M. DiFranco, J. Capote, and J.L. Vergara. 2005. Propagation in the transverse tubular system and voltage dependence of calcium release in normal and mdx mouse muscle fibres. *J. Physiol.* 568:867–880.

Yang, Y.D., H. Cho, J.Y. Koo, M.H. Tak, Y. Cho, W.S. Shim, S.P. Park, J. Lee, B. Lee, B.M. Kim, et al. 2008. TMEM16A confers receptor-activated calcium-dependent chloride conductance. *Nature.* 455:1210–1215. doi:10.1038/nature07313

Zhang, X.D., P.Y. Tseng, and T.Y. Chen. 2008. ATP inhibition of CLC-1 is controlled by oxidation and reduction. *J. Gen. Physiol.* 132:421–428. doi:10.1085/jgp.200810023

Zifarelli, G., and M. Pusch. 2008. The muscle chloride channel ClC-1 is not directly regulated by intracellular ATP. *J. Gen. Physiol.* 131:109–116. doi:10.1085/jgp.200709899